Journal of Materials Science: Materials in Electronics (2018) 29:11509–11520
https://doi.org/10.1007/s10854-018-9246-2

Green synthetic approach of silver nanoparticles from *Bauhinia tomentosa* Linn. leaves extract for potent photocatalytic and in vitro biological applications

K. Ramar[1] · V. Vasanthakumar[2] · A. Priyadharsan[3] · P. Priya[2] · V. Raj[2] · P. M. Anbarasan[3] · R. Vasanthakumari[4] · A. Jafar Ahamed[1]

Received: 17 January 2018 / Accepted: 5 May 2018 / Published online: 22 May 2018

Abstract
Metal nanoparticles have numerous applications such as optics, biomedical sciences, drug delivery, catalysis and electronics. The present work deals with the green synthesis of silver nanoparticles (Ag NPs) using leaves extract of *Bauhinia tomentosa* Linn. and its photocatalytic and in vitro biological activities. The Ag NPs were synthesized via hydrothermal method by adding plant leaf extract. The synthesized Ag NPs were comprehensively characterized by XRD, FTIR, SEM, EDAX and HR-TEM. The green treated Ag NPs have spherical shape with uniform size of 8–25 nm. The optical energy gap of the Ag NPs was determined from the diffuse reflectance spectroscopy. Photocatalytic activity of green treated Ag NPs was studied using an organic dye Rose Bengal under solar irradiation and these nanoparticles showed efficacy in degrading the dye within a few hours of exposure. The detailed in vitro antibacterial and anticancer activities of the green treated Ag NPs were investigated. The Ag NPs was found to have effective antibacterial activity against *Escherichia coli* and *Staphylococcus aureus*. The MTT assay and the microscopic observations of cell morphology revealed, a potent anticancer effects of the synthesized nanoparticles on breast cancer cell line (MCF-7). According to the results, the present reported anisotropic silver nanoparticles with controlled shape and size were synthesized by a simple and efficient method and it has great potential for cost-effective environmental remediation and nanomedicine applications.

1 Introduction

In recent years, nanotechnology has gained major acclaim in different branches of science owing to its multifaceted, beneficial properties including electrical, optical, chemical properties and catalytic properties [1]. Amongst the wide range of available nanoparticles, metal nanoparticles with high specific surface area and a high fraction of surface atoms have been studied extensively because of their exceptional physicochemical characteristics with excellent catalytic activity, optical, electronic, magnetic and biological properties [2].

The properties and function of the nanoparticles are size and shape dependent. Consequently, for a better antibacterial and catalytic activity a specific control over the shape and size of the nanoparticles is prerequisite, which could be achieved by employing different synthesis methods, reducing agents and stabilizers [3, 4]. In current trend of research work, the researchers use plant materials due to their eco-friendly and cost effectiveness material for the synthesis of metal nanoparticles. Though, the synthesis of

V. Vasanthakumar and A. Priyadharsan have equally contributed to this work.

Electronic supplementary material The online version of this article (https://doi.org/10.1007/s10854-018-9246-2) contains supplementary material, which is available to authorized users.

✉ A. Jafar Ahamed
agjafar@yahoo.co.in

[1] PG and Research Department of Chemistry, Jamal Mohamed College (Autonomous), Tiruchirappalli, Tamil Nadu 620 020, India

[2] Advanced Materials Research Laboratory, Department of Chemistry, Periyar University, Salem, Tamil Nadu 636 011, India

[3] Laser Optics and Solar Cell Laboratory, Department of Physics, Periyar University, Salem, Tamil Nadu 636 011, India

[4] Polymer Nano Technology Centre, B.S. Abdur Rahman University, Chennai, Tamil Nadu 60048, India

nanoparticles with uniform size, shape and high crystallinity is an important challenge. A number of chemical and physical approaches available for the synthesis of nanoparticles such as chemical reduction, heat evaporation, solvothermal reduction, photochemical method, electrochemical technique, reverse micelles, microwave assisted methods, sol gel process etc., [5–12]. However, each of these methods has its own limitations, such as long reaction time, formation of nanomaterials of non-uniform shape and size, particle agglomeration, and expensive solvent. Thus, a better alternative is required which can be attained by green synthesis. Green chemistry approach emphasizes the usage of natural organisms which are reliable, simple, nontoxic and eco-friendly [13, 14].

Therefore, researchers in the last few years have turned to hydrothermal method for nanoparticle synthesis [15]. Hydrothermal method became one of the most important methods for preparing nanomaterials due to its advantages of using a simple equipment for obtaining high purity and homogeneity of the product, crystal symmetry, nanoparticles with a narrow size distributions, lower sintering temperature, dense sintered powders, growth of crystals with ultra-low solubility, etc [16]. Therefore, developing new modified hydrothermal green synthesis of metal nanoparticles by the use nontoxic chemicals, environmentally benign solvents, and renewable materials is very necessary.

A survey of earlier literature suggests that leaf extracts from various plants such as *Acalypha indica*, tea leaf, *Ficus carica, Alternanthera sessilis* (Linn.), *Chenopodium murale, Moringa oleifera, Melia dubia, Brassica rapa* L., *Iresine herbstii, Chenopodium murale*, olive leaf, Carica papaya, *Ficus benghalensis*, etc. have been explored for the synthesis of silver nanoparticles [17–28].

Recently, dyes belong to the class of synthetic organic compounds and are widely used in the textile industry. The removal of these non-biodegradable organic chemicals from the environment is a crucial ecological problem [29]. Different methods that are commonly practiced for detoxification of dyes are UV-light degradation, carbon sorption, flocculation and redox treatments. However, these techniques are ineffective and demand a better approach (photocatalytic degradation of dyes). Nowadays biosynthesized nanocatalysts are widely used for the effective removal of dye contaminants [30–33]. In recent years, Ag NPs have been drawing much attention as a new nanomaterial in the emerging field of photocatalyst and antibacterial activity [34]. Ag NPs have the properties of high surface area, very small size (< 20 nm) and high dispersion [35]. These Ag NPs have been incorporated as an efficient antibacterial agent in different applications ranging from disinfecting medical instruments to wastewater treatment. Recent reports suggest that the degradation of organic dyes by Ag NPs is a better choice than the common dye removal methods like redox treatment [36], electro-coagulation [37], carbon sorption [38] and UV photodegradation [39]. Herein, we report for the first time, sunlight illuminated photo-synthesis of silver nanoparticles using aqueous extract of *B. tomentosa* Linn. The acquired silver nanoparticles were exposed to different physico chemical characterization techniques. It was aimed to study the role of *B. tomentosa* Linn. extract in the synthesis of Ag NPs for efficient photocatalytic and in vitro biological applications.

2 Experimental method

2.1 Materials

Silver nitrate ($AgNO_3$) was purchased from Sigma-Aldrich, Mumbai. Rose Bengal was obtained from Merck India Ltd. The leaf samples of *B. tomentosa* Linn. were collected from Madipakkam, Chennai and authenticated by Dr. P. Jayaraman, Director of Plant and Anatomy Research Centre, Chennai (Reg. No. PARC/2016/3238). For the preparation of aqueous extract double distilled water was used.

2.2 Preparation of plant extracts

Healthy leaves of *B. tomentosa* Linn. were procured from the campus and were surface sterilized using double distilled water, then subjected to the experiment. The aqueous extract of leaves was prepared by stirring 5 g of ground samples in 250 ml of distilled water at room temperature for 24 h. The extract was further filtered through Whatman filter paper No. 1 and stored in the refrigerator for further use.

2.3 Preparation of Ag NPs

Ag NPs were synthesized by drop wise addition of 5 ml aqueous *B. tomentosa* Linn. leaf extract to 1 mM silver nitrate solution under vigorous stirring at room temperature for 1 h and there is a change in color of the solution from yellow to reddish. The mixture was then poured into a sealed Teflon-lined autoclave of 100 ml capacity, which was heated and maintained at a temperature of 150 °C for various reaction times (1, 3 and 5 h) and then gradually cooled to room temperature. At last, the nanoparticles were subjected to centrifugation at 10,000 rpm, washed with double distilled water for several times and then dried inside a vacuum dryer at 50 °C to obtain dry powder of green treated Ag NPs.

2.4 Characterization of Ag NPs

Powder X-ray diffraction (PXRD) study was carried out using (Rigaku, Miniflex-600, Japan) X-ray diffractometer [λ (Cu-Kα) = 1.54 Å]. The pattern was recorded with 2θ ranging from

10° with count s^{-1}. The crystalline size was calculated using the Debye–Scherrer's equation. Fourier-Transform Infrared Spectroscopy (FTIR) results were acquired from Jasco 6300 spectrometer (ATR mode) in the range of 400–4000 cm^{-1}. Field Emission Scanning Electron Microscopy (FESEM) images were recorded using a Hitachi SU6600, Japan instrument with an operating voltage of 10 kV equipped with EDAX (EMAX, Horiba 8121-H, Japan). The morphology of the synthesized silver nanoparticles was determined using a High-Resolution Transmission Electron Microscope (Tecnai T-30 G2, D- 905). UV–Vis diffuse reflectance spectra (UV–Vis DRS) were recorded in the range 200–800 nm with a Perkin Elmer Lambda 25 spectrometer. Band gap energy was calculated using Eq. (1)

$$\alpha h\nu = A(h\nu - E_g)^{\eta} \tag{1}$$

where α, $h\nu$, E_g and A are absorption coefficient, light frequency, band gap energy and a proportionality constant respectively, and variable η depends on the nature of the optical transition during photon absorption. For indirect band gap materials, Eg can be estimated from a Tauc plot of $(\alpha h\nu)^2$ versus $h\nu$, with the optical absorption coefficient obtained from the Kubelka–Munk function obtained from Eq. (2) below, by fitting a tangent to band edge

$$\alpha = \frac{(1-R)^2}{2R} \tag{2}$$

2.5 Photocatalytic activity

The photocatalytic activity of these green treated Ag NPs was studied by degradation of RB under solar light irradiation [40]. Prior to the experiment, a suspension was prepared by dissolving 1 mg powder of RB in 100 ml DI water. About 0.5 g of Ag NPs was added to 100 ml dye solution of RB and the mixture was stirred constantly. The solution was allowed to reach an adsorption–desorption equilibrium among the photocatalyst, RB, and water before irradiation. For the evaluation of solar light photocatalytic activity, the colloidal sample was then irradiated with solar light under constant stirring. At regular intervals of time the suspension mixture was taken from the flask, centrifuged and the degradation of RB was monitored using the UV–Vis spectra (UV-2550, Shimadzu). As for the RB aqueous solution with low concentration, its photocatalytic decolorization is a pseudo-first-order reaction and its kinetics may be expressed as $\ln(C/C_0) = -kt$, where k is the apparent rate constant, C_0 and C are the RB concentrations at the initial and after irradiation time (min), respectively [41].

2.6 In vitro biological studies of the green treated Ag NPs

2.6.1 Antibacterial screening

The antibacterial activity of the biosynthesized Ag NPs were investigated against Gram-negative, *Escherichia coli* and Gram-positive, *Staphylococcus aureus* bacterial strains by the agar disc diffusion method [42, 43]. In this process, prior to diffusion inhibition zone tests, all disks and materials were sterilized in an autoclave. Briefly, approximately a 7 mm diameter of a well was made on a Muller Hinton agar plate with the help of gel puncture. The cultures were swabbed on test media with a sterile cotton swab. An equal amount of (25, 50 and 75 μg ml^{-1}) of synthesized particles were inoculated to the well, and the plates were incubated at 37 °C for 24 h. Simultaneously, a standard and the control (without test sample) were also carried out. After incubation period, the diameters of inhibition zones were measured. To optimize the results, the experiment was performed thrice. After the incubation, the antibacterial activity of the biosynthesized Ag NPs was evaluated according to the diameters of the clear inhibition zones.

2.7 Cell viability assay (MTT)

The cell viability was evaluated for MCF-7 human breast cancer cell line via MTT assay to metabolically quantify viable breast cancer cells after exposure to green synthesized of *B. tomentosa* Linn. leaves extract treated Ag NPs. In brief, MCF-7 cells National Centre for Cell Sciences Repository (NCCS, Pune, India) were seeded into 96-well plates with concentration of 1×10^4 cells $well^{-1}$ in DMEM media with antibiotic antimycotic solution and 10% fetal bovine serum (Himedia, India) and cultured in a humidified incubator at 37 °C with 5% CO_2 for 24 h. After treatment period the medium was replaced with various test concentration of Ag NPs (25, 50, 100, 250 and 500 μg ml^{-1}). The control cells were incubated with a fresh culture medium. Following a further incubation for 48 h, the MTT reagent (final concentration being 0.5 mg ml^{-1}) was added to each well and incubated for 4 h to detect the metabolically active cells. Finally, the formed crystals was dissolved with 100 μl of DMSO and thoroughly mixed. The absorbance of each well was measured at 570 nm by a microplate reader and the percentage of cell viability was calculated using the Eq. (3). The results were obtained from triplicate determinations. The cytomorphological changes of MCF-7 cells were also investigated by optical microscopy. Morphologies of the cell lines to NPs were compared by phase contrast microscopy.

$$\text{Cell viability}(\%) = (\text{OD of sample}) \times 100/(\text{OD of untreated control}) \tag{3}$$

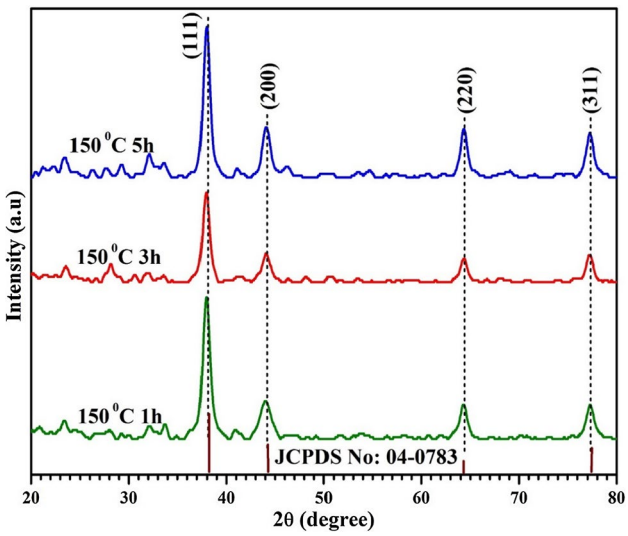

Fig. 1 XRD pattern of synthesized Ag NPs with *B. tomentosa* leaves extract

3 Results and discussion

3.1 X-ray diffraction (XRD)

The XRD pattern of the prepared Ag NPs are as shown in Fig. 1. Four diffraction peaks have shown the planes of face centered cubic (FCC) silver at 38.1° (111), 44.1° (200), 64.3° (220) and 77.1° (311) respectively. The peaks of Ag NPs are in good agreement with reference to the unit cell of the face centered cubic structure (JCPDS File No: 04-0783) with a lattice parameter of a = 4.086 Å. X-ray diffraction results clearly show that the Ag NPs formed by the reduction of Ag^+ ions by the *B. tomentosa* leaf extract are crystalline in nature. The relative intensity of the (200) plane to (111) diffraction peaks in the figure was higher than the conservative value. This shows that the as prepared Ag NPs may be enhanced in (111) facets and thus the (111) plane appears to be preferentially concerned with parallel to the surface of the aiding substrate [44]. Meanwhile, the size of these particles could be expected from the Debye–Scherrer Eq. (4) by determining the width of the (111) Bragg reflection [45].

$$D = \frac{K\lambda}{\beta \cos\theta} \tag{4}$$

where D is mean size of crystalline domains which may be smaller or equal to the grain size, K is dimensionless shape factor with a value close to unity, λ is the wavelength of the X-ray source (0.1541 nm) used in XRD, β is line broadening at full width half maximum intensity (FWHM) and θ is the Bragg angle (in degrees). From the Scherrer equation the average crystallite size of silver nanoparticles is found to be 20 nm. The particle sizes obtained from XRD are 17.4, 20.7 and 22.2 nm. The XRD patterns showed in this work are in good agreement with the previous research reported for green synthesis of Ag NPs [46].

3.2 Fourier transform infrared spectroscopy (FTIR)

The FT-IR spectrum of green treated Ag NPs by the *B. tomentosa* leaves extract is shown in Fig. 2. Strong absorption peaks at 3309 and 3421 cm^{-1} result from stretching of the –NH band of amino groups or is suggestive of bonded –OH hydroxyl group. The intense band appearing at 1721 cm^{-1} is assigned for –CO stretching mode showing the presence of –COOH group in the reducing agent. The band at 1443 cm^{-1} may be due to the C–O–H vibrations [47]. The FT-IR spectrum also shows bands at 1608 and 1558 cm^{-1} identified the amide I and amide II arising due to carbonyl stretch and –N–H stretch vibrations in the amide linkages of the proteins, respectively. The carboxyl (–C=O), hydroxyl (–OH), and amine (N–H) groups in *B. tomentosa* leaf extract are primarily involved in reduction of Ag^+ ions to Ag^0 nanoparticles. The carbonyl group of amino acid remains a strong binding ability with silver, signifying the formation of a layer covering silver nanoparticles and acting as a capping agent to forbid agglomeration and lend stability to the medium. These results confirm the presence of possible proteins acting as reducing and stabilizing agents.

3.3 SEM, EDAX and HR-TEM analysis

The surface morphology of the hydrothermally synthesized Ag NPs at various durations (150 °C t = 1, 3 and 5 h)

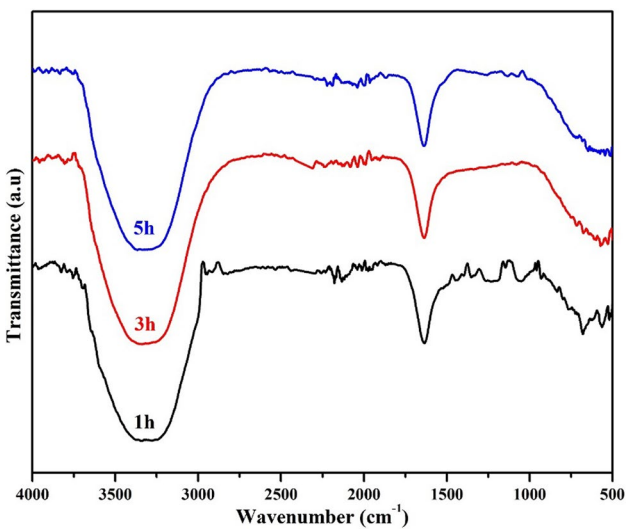

Fig. 2 FT-IR spectra of green treated Ag NPs by *B. tomentosa* leaves extract at different hours

was investigated by SEM. It is clearly seen from the SEM images (Fig. 3a–f) that the morphology of all of the synthesized nanomaterials are agglomerated with higher density of polydispersed. The EDAX analysis of green treated Ag NPs with respective SEM images are shown in Fig. 4. The results confirmed the presence of elements Ag (52.59%), O (24.50%) and C (14.18%) with strong peaks. The C and O signals are attributed mainly to the biomolecules in the *B. tomentosa* leaves extract [35]. The EDAX analysis thus confirmed presence of elemental silver as major constituents which if successful conjugation of *B. tomentosa* Linn. on silver nanoparticles.

The average diameter of the green treated nanoparticles at different time based on the analyses of TEM images are shown in Fig. 5. From the images we could observe that the synthesized nanoparticles are well dispersed, mostly spherical in shape with smooth edges and the average diameter of silver nanoparticles can be considerably adjusted by varying reaction time from 1 to 5 h, The approximate particles size in the range of 8–25 nm were obtained for a reaction time of 1 h (Fig. 5a, b). On increasing the reaction time to 3 h, the resulted particles are larger in size (25–40 nm) and are mostly fused together (Fig. 5c). The same way, a further increase in reaction time, the obtained nanoparticles are well dispersed and the average diameter of silver nanoparticles obviously increased from 40 to 50 nm with time of 5 h (Fig. 5d). The lattice spacing of the nanoparticle is 2.8 nm which is clearly shown in Fig. 5f. The observed increase in particle size as increasing the reaction time, it could be due to the fact that, biomolecules present in *B. tomentosa* Linn. have adhered to the surface of the nanoparticles. The crystalline nature of the green treated Ag NPs was confirmed by the Selected Area Electron Diffraction (SAED) (Fig. 5f) which showed the well-defined quasi-ring-like diffraction pattern (111, 200), (220, 311), demonstrating that the crystalline structure was formed, which is ascribed to XRD pattern [36, 37].

3.4 UV–Vis diffused reflectance spectroscopy

UV–Vis diffuse reflectance spectra (DRS) are used to determine the optical properties of the Ag NPs. Figure 6 shows the absorption spectra of Ag NPs recorded in the range 200–800 nm. In the UV-DRS spectra, the optical absorption

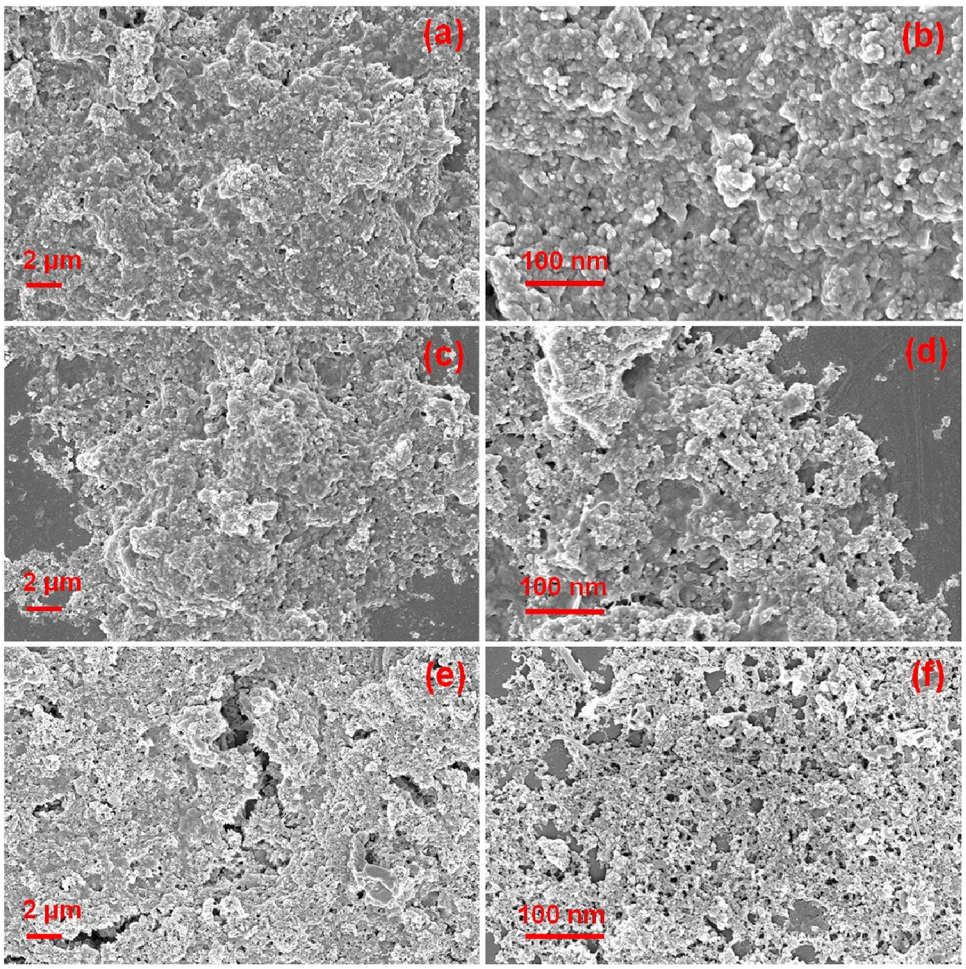

Fig. 3 FE-SEM images of green treated Ag NPs with different magnification at different hours **a, b** 1 h; **c, d** 3 h and **e, f** 5 h

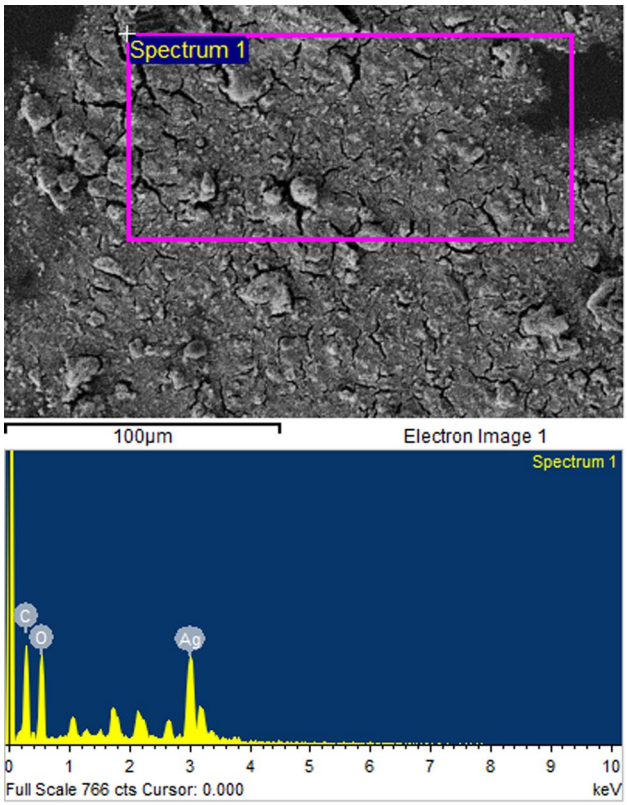

Fig. 4 EDAX analysis of green treated Ag NPs

edge shifts to higher wavelength region with the increase of 150 °C at 5 h and observed red shift in Ag NPs. Furthermore, the band gap energy could be calculated from the Tauc plot $[(\alpha h\nu)^{0.5}]$ versus photon energy $(h\nu)$ for the indirect energy gap semiconductor, as shown in Fig. 6, inset. The band gap energies of Ag NPs are estimated to be 1.92, 1.99 and 2.09 eV for the 1 h (150 °C), 3 h (150 °C) and 5 h (150 °C) respectively. This suggests that the minimum energy required to excite an electron from the valence band to the conduction band will be considerably lower in 5 h (150 °C) Ag NPs and it has a larger redox potential for the photocatalytic decomposition of organic contaminants under visible irradiation.

3.5 Photocatalytic performance

Photocatalysis is widely used in environmental remediation; often the goal in this application of metal nanoparticles is to catalyze some reactions that are differently unfeasible. It is well-known that the catalytic performance of nanoparticles is intensely dependent on its distribution, size and shape. Usually, a superior surface-to-volume ratio is given to show a higher catalytic activity [48]. It is a well-known fact that Ag NPs show better catalytic activity on dye reduction and removal. As shown in Fig. 7a, Ag NPs sample performed a much greater degradation ability. Initially, there is almost no degradation as the solution is without any catalyst under

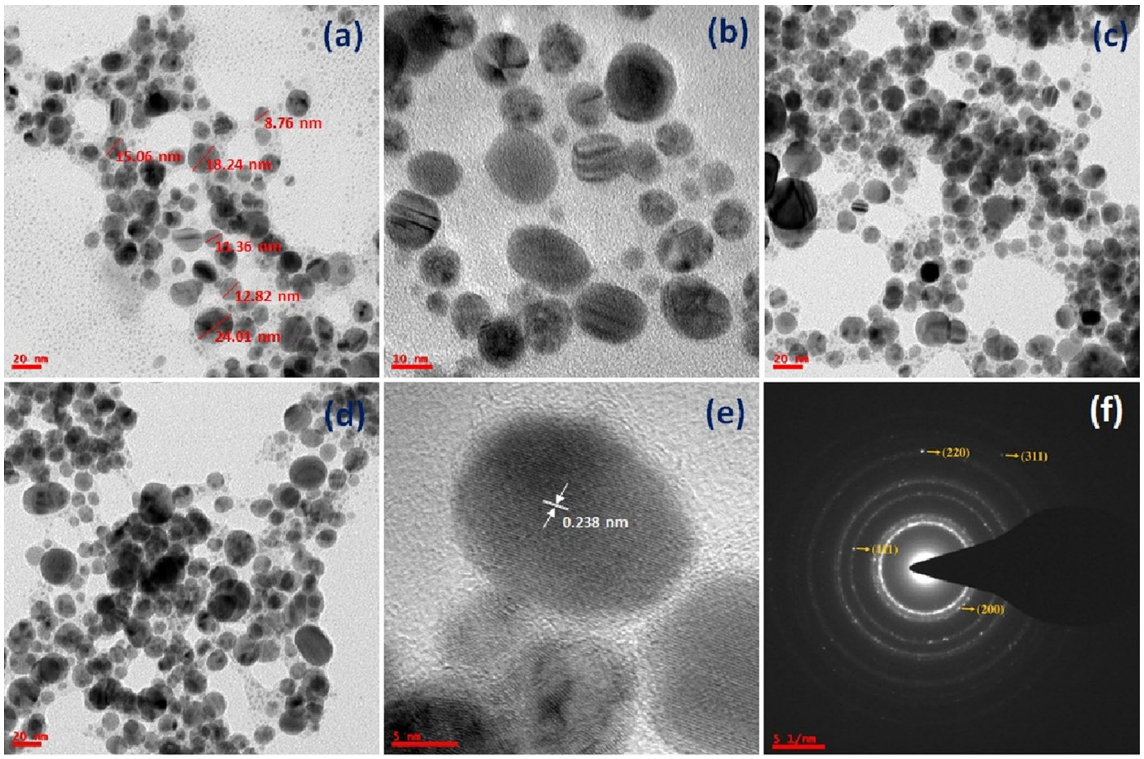

Fig. 5 TEM images of Ag NPs obtained at 150 °C for **a, b** 1 h; **c** 3 h, **d** 5 h, **e** lattice fringes and **f** selected area electron diffraction pattern

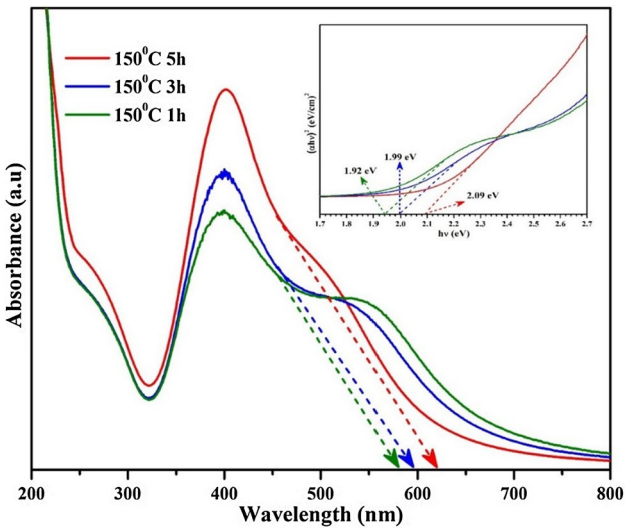

Fig. 6 UV-DRS spectrum for the Ag NPs, inset: tauc plot of Ag NPs synthesized at various time (1, 3 and 5 h)

solar light irradiation. The catalytic degradation of the dye in the presence of Ag NPs was identified visually by the change in colour. After irradiation for 20 min, the photodegradation rate of the RB solution reached about 100%, indicating that RB was hardly completely degraded. This showed that the green synthesis of Ag NPs enhance the photocatalytic activity. The photocatalytic activity of as prepared Ag NPs was compared to the earlier reported solar light activity of various nanoparticles as shown in Table 1. From Table 1, it is clear that the Ag NPs catalyst exhibited better visible-light activity compared to the previously reported results of other nanoparticles.

Figure 7b shows photodegradation of RB under different circumstances. The y-axis of degradation was proclaimed as C_t/C_0. C_t is the remaining content of RB after different irradiation time. C_0 is the initial content of RB. The photocatalytic degradation of RB followed pseudo-first order kinetics (Fig. 7c) [54]. The rate constant (k) without catalyst and with Ag NPs are 0.0003 and 0.1532 min^{-1} with high correlation coefficient (R^2) of 0.9724, indicating the photocatalytic behavior of green treated Ag NPs obeyed the pseudo-first order reaction dynamics model. To check the stability, three succeeding cycles of photocatalytic degradation of RB was conducted using Ag NPs, and the results are shown in Fig. 7d. The photocatalytic activity of Ag NPs was retained during three cycles signifying that the photocatalyst has outstanding stability. The change in efficiency is be attributed to the loss of catalyst during reuse. There may be a question of stability of the catalyst after reuse; the catalyst was also observed under XRD and FTIR after three catalytic cycles. It can be ascertained experiential that there is no change in the diffraction peaks of the catalyst compared to that of virgin one as shown in Figs. S1, S2. The auspicious characteristics of Ag NPs in terms of photocatalytic activity and stability make it pretty for numerous indoor applications and for the removal of other volatile organic compounds too. The mechanism of the photocatalytic degradation of RB dye by Ag NPs is given as following Eqs. (5–10).

$$\text{Dye} + \text{Solar light} \rightarrow \text{Dye}^{*} \quad (5)$$

$$\text{Dye}^{*} + \text{Ag NPs} \rightarrow \text{Dye}^{\bullet+} + \text{Ag}\,(e^{-}) \quad (6)$$

$$\text{Ag}\,(e^{-}) + O_2 \rightarrow O_2^{\bullet-} \quad (7)$$

$$O_2^{\bullet-} + H^{+} \rightarrow HO_2^{\bullet} \quad (8)$$

$$HO_2^{\bullet} + H^{+} \rightarrow HO^{\bullet} + OH^{-} \quad (9)$$

$$\text{Dye}^{\bullet+} + \text{Reactive oxygenated radical} \rightarrow \text{Degraded products} \quad (10)$$

3.6 Antimicrobial activity

The antibacterial activity of the biosynthesized Ag NPs was determined by using the diffusion inhibition zone method at four different concentrations (such as 25, 50 and 75 μg ml^{-1}) using ciprofloxacin as a standard antibiotic. The Ag NPs have good inhibition against the growth of pathogenic bacterial strain and the test results shown in Fig. 8 and experimentally obtained diameters of inhibition zones were measured and presented in Table 2. Based on above experimental results, we found that biosynthesized Ag NPs exhibited excellent antibacterial effects against *E. coli* and *S. aureus* and the antibacterial activity is increased with increases of concentration of Ag–NPs. However, they were less effective against *E. coli* than against *S. aureus* and this phenomenon was attributed to the different structure of the cell walls of bacteria. generally accepted that the antibacterial activities are realized by the interaction between nanoparticles and bacteria occurs through initial adhesion, accumulation of nanoparticles on the bacterial cell wall, alteration/perforation of the cell wall and finally penetration of nanoparticles inside the cell leading to cell death.

3.7 Anticancer activity of Ag NPs

The cytotoxic effects of *B. tomentosa* Linn. Leaves extract treated Ag NPs against MCF-7 breast cancer cells were evaluated using the MTT assay. A comprehensive MTT assay revealed, significant differences in the viability of MCF-7 cells in the presence of different concentrations (25, 50, 100, 250 and 500 μg ml^{-1}) of green synthesized silver nanoparticles and the enhancement of cytotoxic activity with the increase of silver nanoparticle concentration (Fig. 9). At the best condition, the maximum cell mortality of 42.2% was obtained to the exposure of 500 μg ml^{-1} of green synthesized Ag NPs. Figure 10

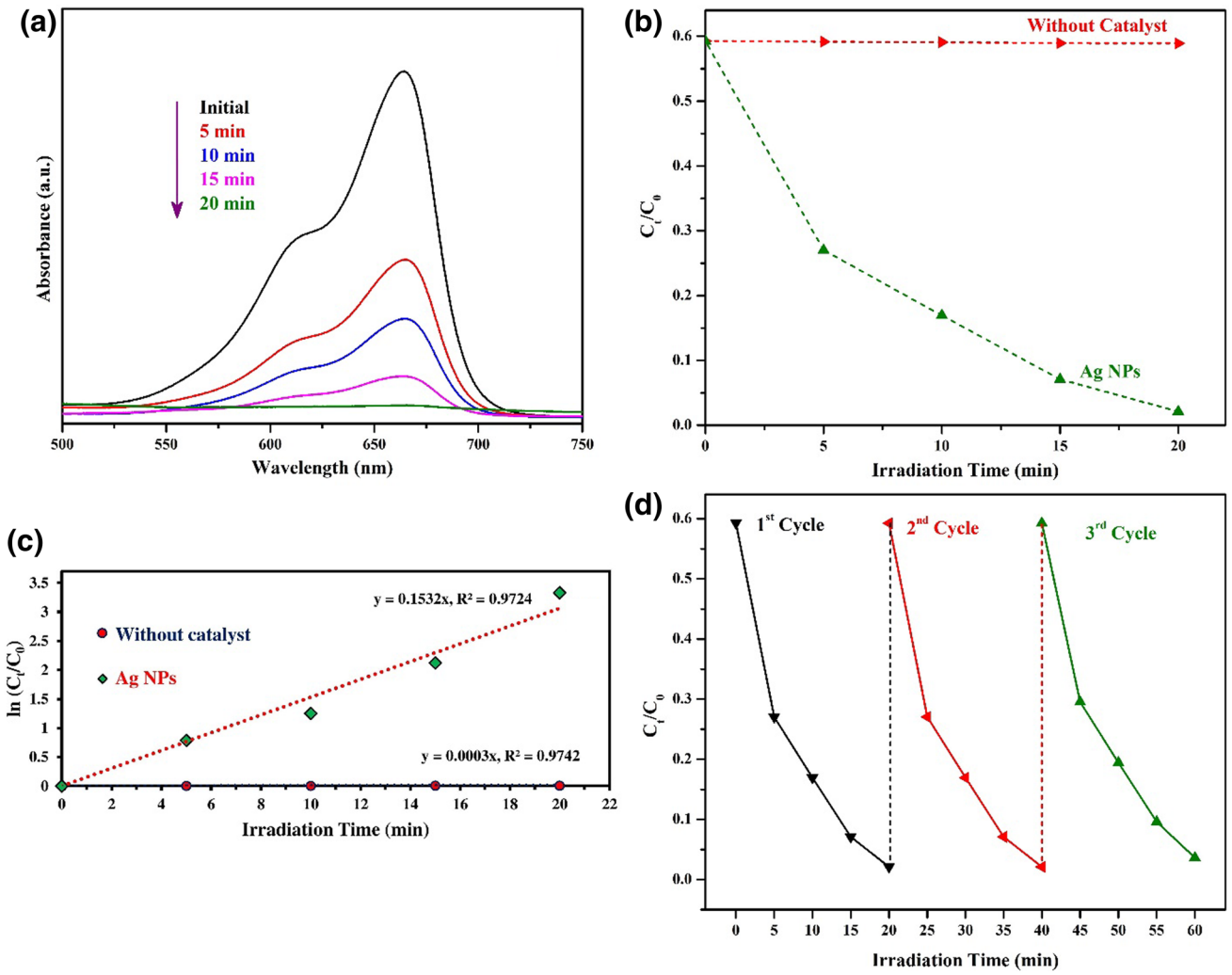

Fig. 7 **a** Absorption spectra of the RB solution in the presence of Ag NPs, **b** photocatalytic decomposition rates of RB dye, **c** kinetic linear fitting curves of RB over blank and Ag NPs samples, **d** cycling degradation curve for Ag NPs

Table 1 Comparison of solar light degradation rate (%) of RB over previously reported nanoparticles

Catalyst	% Removal	Catalyst ($g\ l^{-1}$)	Irradiation time (min)	References
Ag_2S NPs	92	2.0	30	[49]
Ag_2S@ Ag_2CO_3	95	0.5	60	[50]
TiO_2 NPs	100	0.2	120	[51]
Ag/AgBr/ CNTs	79	0.2	60	[52]
AgBr/TiO_2	95	2.5	840	[53]
Ag NPs	100	0.5	20	Present work

shows the optical microscopic studies showing differences in morphology of MCF-7 breast cancer cell lines in presence of Ag NPs, as rising the concentration of green treated Ag NPs with nanospheres, cell rounding zone was extended, detachment and finally the cell clumping and death was clearly observed and these superior cytotoxic activity is due to the non-toxic and biocompatibility of the metal nanostructures. Their anticancer activity could be attributed to the adsorbed organic compounds of *B. tomentosa* Linn. leaves extracts on their surface. In the other words, encapsulation of Ag NPs with *B. tomentosa* Linn. leaves extracts led to the development of a biogenic nonocarrier with significant anticancer activity on various tumors. These simple, cost-effective and eco-friendly green treated Ag NPs seem to be potential for interactions with tumor cells and novel targeted cancer therapy using nanomedicine approach.

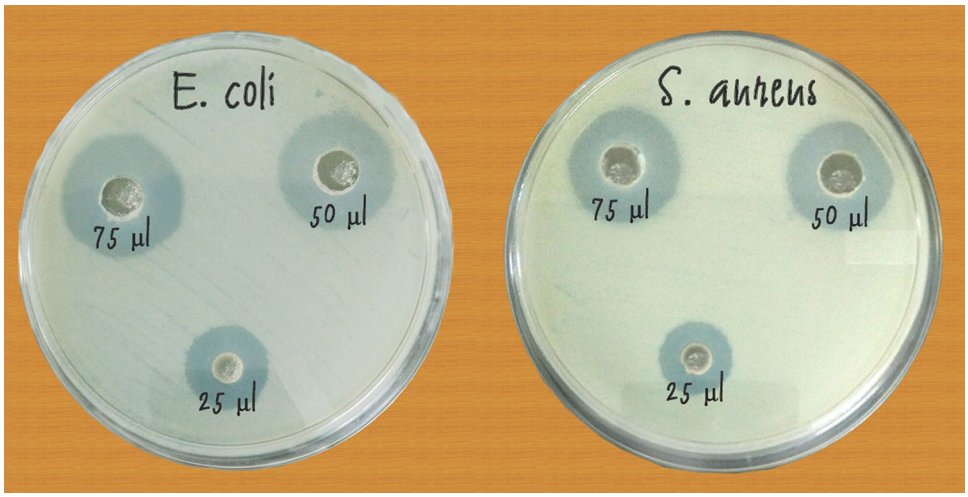

Fig. 8 Antibacterial activity of Ag NPs towards Gram-negative (*E. coli*) and Gram-positive (*S. aureus*) bacteria

Table 2 Antibacterial activity of the catalysts against two human pathogenic bacteria

Nanoparticle	Bacterial strain	Zone of inhibition level (in mm) (mean value of four measurements)			Standard 5 µl
		25 µl	50 µl	75 µl	
AgNPs	*E. coli*	11.4 ± 1.2	18.3 ± 3.5	23.6 ± 1.4	29.00 ± 2.0
	S. aureus	12.7 ± 1.4	17.1 ± 2.4	22.5 ± 1.2	30.23 ± 1.6

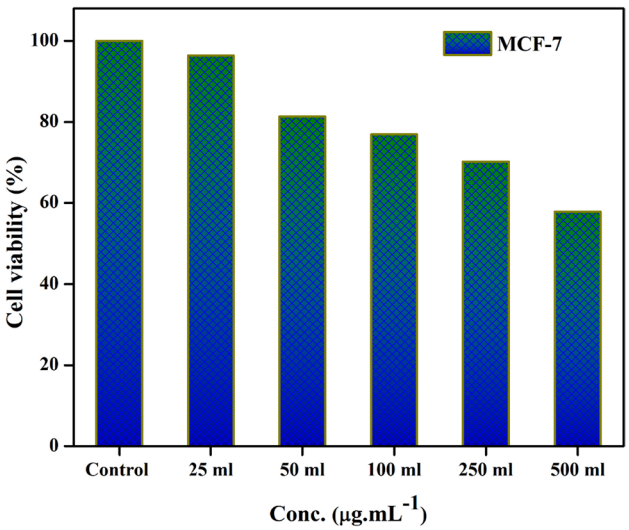

Fig. 9 Cell viability of concentration dependent Ag NPs against MCF-7 cancer cell lines

4 Conclusions

The present study envisages a green approach to the synthesis of Ag NPs by using *B. tomentosa* Linn. leaves extract at different times (1, 3 and 5 h) of reaction at 150 °C. The obtained green treated Ag NPs are nanocrystalline in nature are mostly spherical in shape and the average diameters of the particles size 8–25, 25–40 and 40–50 nm for the reaction times of 1, 3 and 5 h respectively. On the other hand, the present study establishes that the Ag nanoparticles reveal photocatalytic activity and can be used in water purification system and other industrial purposes. Furthermore the Ag NPs were an excellent antibacterial activity against Gram-positive and Gram-negative bacterial strains. Further we observed that the green treated Ag NPs have potent anticancer activity against breast cancer cell line (MCF-7). In conclusion, the silver nanoparticles synthesized using *B. tomentosa* Linn. plant sources might be a potential agent for the environmental remediation and biomedical application via simple and cost effective manner.

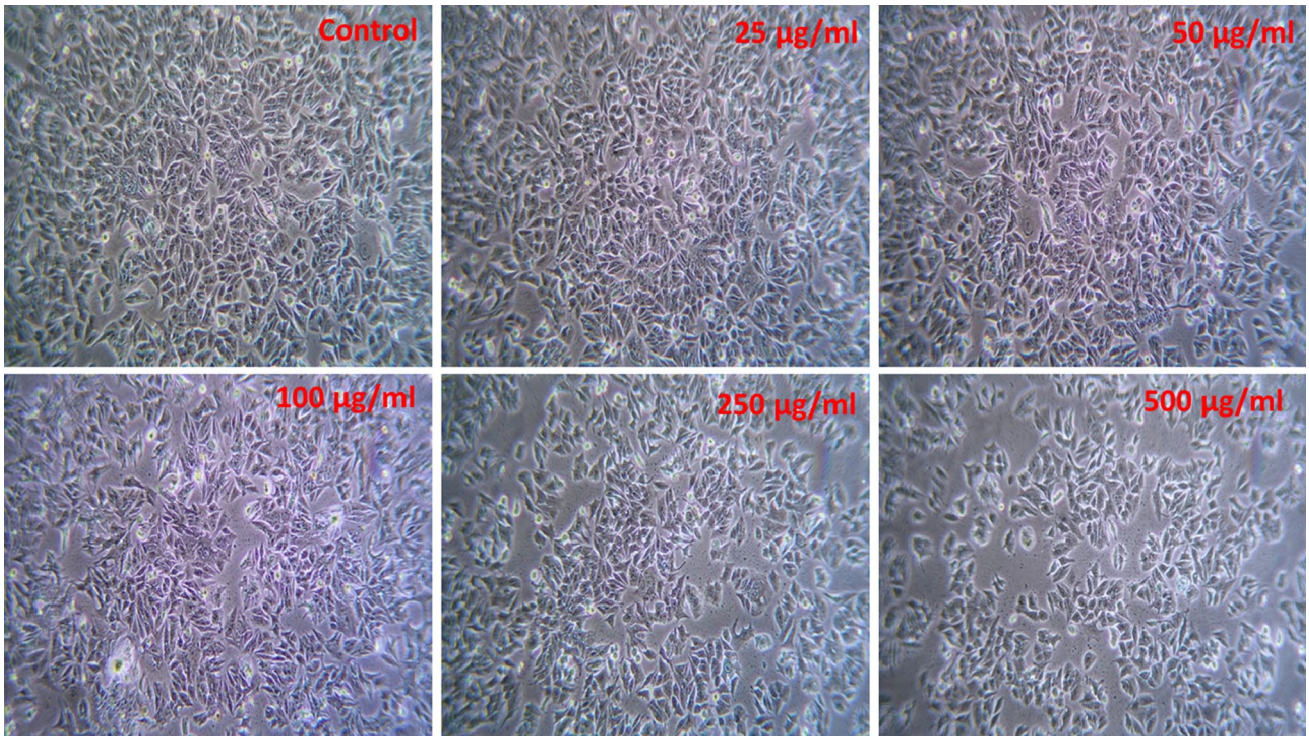

Fig. 10 Morphology changes of MCF-7 cancer cell lines after treatment with green treated Ag NPs

Acknowledgements Special thanks are due to B.S. Abdur Rahman University, Chennai for providing laboratory facilities to carry out this study, NCNSNT, University of Madras, Chennai and Royal Bio Research Centre, Chennai for providing necessary facilities for completing the present study.

Compliance with ethical standards

Conflict of interest There are no conflicts to declare.

References

1. R. Vaidyanathan, K. Kalishwaralal, S. Gopalram, S. Gurunathan, Nanosilver-the burgeoning therapeutic molecule and its green synthesis. Biotechnol. Adv. **27**, 924–937 (2009). https://doi.org/10.1016/j.biotechadv.2009.08.001
2. M. Catauro, M.G. Raucci, F.D.E. Gaetano, A. Marotta, Antibacterial and bioactive silver-containing $Na_2O{\cdot}CaO{\cdot}2SiO_2$ glass prepared by sol-gel method. J. Mater. Sci. Mater. Med. **5**, 831–837 (2004). https://doi.org/10.1023/B:JMSM.0000032825.51052.00
3. R.J. Chimentão, I. Kirm, F. Medina, X. Rodríguez, Y. Cesteros, P. Salagre, J.E. Sueiras, Different morphologies of silver nanoparticles as catalysts for the selective oxidation of styrene in the gas phase. Chem. Commun. (Camb). **7**, 846–847 (2004). https://doi.org/10.1039/b400762j
4. S.Y. Yeo, H.J.O.O. Lee, S.H. Jeong, Preparation of nanocomposite bers for permanent antibacterial effect. J. Mater. Sci. **38**, 2143–2147 (2003). https://doi.org/10.1023/A:1023767828656
5. Y. Liguo, Z. Yanhua, Preparation of nano-silver flake by chemical reduction method. Rare Met. Mater. Eng. **39**, 401–404 (2010). https://doi.org/10.1016/S1875-5372(10)60088-4
6. S. Iravani, H. Korbekandi, S.V. Mirmohammadi, B. Zolfaghari Synthesis of silver nanoparticles: chemical, physical and biological methods. Res. Pharm. Sci. **9** 385–406 (2014)
7. Y. Yang, Z. Huang, D. Li, M. Nogami, Solvothermal synthesis of platinum nanoparticles and their SERS properties. J. Phys. Chem. C **111**, 76580H (2010). https://doi.org/10.1117/12.867958
8. V. Babaahmadi, M. Montazer, T. Toliyat, M. Ghanbarafjeh, Photochemical reduction of silver nitrate to nano silver using stannous chloride, Ctab, nanomater. Appl. Prop. **1**, 183–190 (2011)
9. R.a.. Khaydarov, R.R. Khaydarov, O. Gapurova, Y. Estrin, T. Scheper, Electrochemical method for the synthesis of silver nanoparticles. J. Nanoparticle Res. **11**, 1193–1200 (2008). https://doi.org/10.1007/s11051-008-9513-x
10. T.T.N. Dung, N.Q. Buu, D.V. Quang, H.T. Ha, L.A. Bang, N.H. Chau, N.T. Ly, N.V. Trung, Synthesis of nanosilver particles by reverse micelle method and study of their bactericidal properties. J. Phys. Conf. Ser. **187**, 12054 (2009). https://doi.org/10.1088/1742-6596/187/1/012054
11. G. Xu, S. Gao, X. Ji, X. Zhang, Characterization and synthesis mechanism of nanosilver/PAMPS composites by microwave. Soft Nanosci. Lett. **4**, 15–23 (2014)
12. N. Lkhagvajav, I. Yasa, E. Celik, M. Koizhaiganova, O. Sari, Antimicrobial activity of colloidal silver nanoparticles prepared by sol-gel method. Dig. J. Nanomater. Biostruct. **6**, 149–154 (2011)
13. K.B. Narayanan, N. Sakthivel, Biological synthesis of metal nanoparticles by microbes. Adv. Colloid Interface Sci. **156**, 1–13 (2010). https://doi.org/10.1016/j.cis.2010.02.001
14. A. Saxena, R.M. Tripathi, R.P. Singh, Biological synthesis of silver nanoparticles by using onion (*Allium cepa*) extract and their antibacterial activity. Dig. J. Nanomater. Bios. **5**, 427–432 (2010)

15. Y. Wang, J. Yu, W. Xiao, Q. Li, Microwave-assisted hydrothermal synthesis of graphene based Au–TiO_2 photocatalysts for efficient visible-light hydrogen production. J. Mater. Chem. A **2**, 3847 (2014). https://doi.org/10.1039/c3ta14908k
16. I. Ocsoy, A. Demirbas, E.S. McLamore, B. Altinsoy, N. Ildiz, A. Baldemir, Green synthesis with incorporated hydrothermal approaches for silver nanoparticles formation and enhanced antimicrobial activity against bacterial and fungal pathogens. J. Mol. Liq. **238**, 263–269 (2017). https://doi.org/10.1016/j.molliq.2017.05.012
17. R.R. Banala, V.B. Nagati, P.R. Karnati, Green synthesis and characterization of Carica papaya leaf extract coated silver nanoparticles through X-ray diffraction, electron microscopy and evaluation of bactericidal properties. Saudi J. Biol. Sci. **22**, 637–644 (2015). https://doi.org/10.1016/j.sjbs.2015.01.007
18. M.S. Abdel-Aziz, M.S. Shaheen, A.A. El-Nekeety, M.A. Abdel-Wahhab, Antioxidant and antibacterial activity of silver nanoparticles biosynthesized using *Chenopodium murale* leaf extract. J. Saudi Chem. Soc. **18**, 356–363 (2014). https://doi.org/10.1016/j.jscs.2013.09.011
19. A. Saxena, R.M. Tripathi, F. Zafar, P. Singh, Green synthesis of silver nanoparticles using aqueous solution of *Ficus benghalensis* leaf extract and characterization of their antibacterial activity. Mater. Lett. **67**, 91–94 (2012). https://doi.org/10.1016/j.matlet.2011.09.038
20. B. Ulug, M. Haluk Turkdemir, A. Cicek, A. Mete, Role of irradiation in the green synthesis of silver nanoparticles mediated by fig (*Ficus carica*) leaf extract. Spectrochim. Acta A **135**, 153–161 (2015). https://doi.org/10.1016/j.saa.2014.06.142
21. C. Dipankar, S. Murugan, The green synthesis, characterization and evaluation of the biological activities of silver nanoparticles synthesized from Iresine herbstii leaf aqueous extracts. Colloids Surfaces B **98**, 112–119 (2012). https://doi.org/10.1016/j.colsurfb.2012.04.006
22. V. Kathiravan, S. Ravi, S. Ashokkumar, Synthesis of silver nanoparticles from *Melia dubia* leaf extract and their in vitro anticancer activity. Spectrochim. Acta A **130**, 116–121 (2014). https://doi.org/10.1016/j.saa.2014.03.107
23. T.N.V.K.V. Prasad, E.K. Elumalai, Biofabrication of Ag nanoparticles using *Moringa oleifera* leaf extract and their antimicrobial activity. Asian Pac. J. Trop. Biomed. **1**, 439–442 (2011). https://doi.org/10.1016/S2221-1691(11)60096-8
24. M.M.H. Khalil, E.H. Ismail, K.Z. El-Baghdady, D. Mohamed, Green synthesis of silver nanoparticles using olive leaf extract and its antibacterial activity. Arab J. Chem. **7**, 1131–1139 (2014). https://doi.org/10.1016/j.arabjc.2013.04.007
25. Q. Sun, X. Cai, J. Li, M. Zheng, Z. Chen, C.P. Yu, Green synthesis of silver nanoparticles using tea leaf extract and evaluation of their stability and antibacterial activity. Colloids Surfaces A **444**, 226–231 (2014). https://doi.org/10.1016/j.colsurfa.2013.12.065
26. C. Krishnaraj, E.G. Jagan, S. Rajasekar, P. Selvakumar, P.T. Kalaichelvan, N. Mohan, Synthesis of silver nanoparticles using *Acalypha indica* leaf extracts and its antibacterial activity against water borne pathogens. Colloids Surfaces B **76**, 50–56 (2010). https://doi.org/10.1016/j.colsurfb.2009.10.008
27. K.L. Niraimathi, V. Sudha, R. Lavanya, P. Brindha, Biosynthesis of silver nanoparticles using *Alternanthera sessilis* (Linn.) extract and their antimicrobial, antioxidant activities. Colloids Surfaces B **102**, 288–291 (2013). https://doi.org/10.1016/j.colsurfb.2012.08.041
28. K.B. Narayanan, H.H. Park, Antifungal activity of silver nanoparticles synthesized using turnip leaf extract (*Brassica rapa* L.) against wood rotting pathogens. Eur. J. Plant Pathol. **140**, 185–192 (2014). https://doi.org/10.1007/s10658-014-0399-4
29. S. Shanavas, A. Priyadharsan, V. Vasanthakumar, A. Arunkumar, P.M. Anbarasan, S. Bharathkumar, Mechanistic investigation of visible light driven novel La_2CuO_4/CeO_2/rGO ternary hybrid nanocomposites for enhanced photocatalytic performance and antibacterial activity. J. Photochem. Photobiol. A **340**, 96–108 (2017). https://doi.org/10.1016/j.jphotochem.2017.03.002
30. J. Saha, A. Begum, A. Mukherjee, S. Kumar, A novel green synthesis of silver nanoparticles and their catalytic action in reduction of methylene blue dye. Sustain. Environ. Res. **27**, 245–250 (2017). https://doi.org/10.1016/j.serj.2017.04.003
31. H. Veisi, S. Azizi, P. Mohammadi, Green synthesis of the silver nanoparticles mediated by *Thymbra spicata* extract and its application as a heterogeneous and recyclable nanocatalyst for catalytic reduction of a variety of dyes in water. J. Clean. Prod. **170**, 1536–1543 (2018). https://doi.org/10.1016/j.jclepro.2017.09.265
32. R. Arunachalam, S. Dhanasingh, B. Kalimuthu, M. Uthirappan, C. Rose, A.B. Mandal, Phytosynthesis of silver nanoparticles using *Coccinia grandis* leaf extract and its application in the photocatalytic degradation. Colloids Surfaces B **94**, 226–230 (2012). https://doi.org/10.1016/j.colsurfb.2012.01.040
33. T. Varadavenkatesan, R. Selvaraj, R. Vinayagam, Phyto-synthesis of silver nanoparticles from *Mussaenda erythrophylla* leaf extract and their application in catalytic degradation of methyl orange dye. J. Mol. Liq. **221**, 1063–1070 (2016). https://doi.org/10.1016/j.molliq.2016.06.064
34. N. Muniyappan, N.S. Nagarajan, Green synthesis of silver nanoparticles with *Dalbergia spinosa* leaves and their applications in biological and catalytic activities. Process Biochem. **49**, 1054–1061 (2014). https://doi.org/10.1016/j.procbio.2014.03.015
35. T.V. Mathew, S. Kuriakose, Studies on the antimicrobial properties of colloidal silver nanoparticles stabilized by bovine serum albumin. Colloids Surfaces B **101**, 14–18 (2013). https://doi.org/10.1016/j.colsurfb.2012.05.017
36. Y.H. Kim, R. Hensley, Effective control of chlorination and dechlorination at wastewater treatment plants using redox potential. Water Environ. Res. **69**, 1008–1014 (1995)
37. L. Szpyrkowicz, S.N. Kaul, R.N. Neti, Tannery wastewater treatment by electro-oxidation coupled with a biological process. J. Appl. Electrochem. **35**, 381–390 (2005). https://doi.org/10.1007/s10800-005-0796-7
38. N. Gomez, S. Chen, C.E. Schmidt, Polarization of hippocampal neurons with competitive surface stimuli: contact guidance cues are preferred over chemical ligands. J. R. Soc. Interface. **4**, 223–233 (2007). https://doi.org/10.1098/rsif.2006.0171
39. M.R. Sohrabi, M. Ghavami, Photocatalytic degradation of direct red 23 dye using UV/TiO_2: effect of operational parameters. J. Hazard. Mater. **153**, 1235–1239 (2008). https://doi.org/10.1016/j.jhazmat.2007.09.114
40. X. Wang, S. Li, H. Yu, J. Yu, In situ anion-exchange synthesis and photocatalytic activity of $Ag_8W_4O_{16}$/AgCl-nanoparticle core–shell nanorods. J. Mol. Catal. A **334**, 52–59 (2011). https://doi.org/10.1016/j.molcata.2010.10.022
41. A. Priyadharsan, V. Vasanthakumar, S. Karthikeyan, V. Raj, S. Shanavas, P.M. Anbarasan, Multi-functional properties of ternary CeO_2/SnO_2/rGO nanocomposites: visible light driven photocatalyst and heavy metal removal. J. Photochem. Photobiol. A **346**, 32–45 (2017). https://doi.org/10.1016/j.jphotochem.2017.05.030
42. M.A.R. Ahamed, D. Jeyakumar, A.R. Burkanudeen, Removal of cations using ion-binding terpolymer involving 2-amino-6-nitrobenzothiazole and thiosemicarbazide with formaldehyde by batch equilibrium technique. J. Hazard. Mater. **248–249**, 59–68 (2013). https://doi.org/10.1016/j.jhazmat.2012.12.047
43. V. Vasanthakumar, A. Saranya, A. Raja, S. Prakash, V. Anbarasu, P. Priya, V. Raj, The synthesis, characterization, removal of toxic metal ions and in vitro biological applications of a sulfanilamide–salicylic acid–formaldehyde terpolymer. RSC Adv. **6**, 54904–54917 (2016). https://doi.org/10.1039/C6RA05115D

44. V. Germain, J. Li, D. Ingert, Z.L. Wang, M.P. Pileni, Stacking faults in formation of silver nanodisks. J. Phys. Chem. B. **107**, 8717–8720 (2003). https://doi.org/10.1021/jp0303826
45. H. Borchert, E.V. Shevchenko, A. Robert, I. Mekis, A. Kornowski, G. Grübel, H. Weller, Determination of nanocrystal sizes: a comparison of TEM, SAXS, and XRD studies of highly monodisperse CoPt 3 particles. Langmuir **21**, 1931–1936 (2005) https://doi.org/10.1021/la0477183
46. P. Kouvaris, A. Delimitis, V. Zaspalis, D. Papadopoulos, S.A. Tsipas, N. Michailidis, Green synthesis and characterization of silver nanoparticles produced using *Arbutus unedo* leaf extract. Mater. Lett. **76**, 18–20 (2012). https://doi.org/10.1016/j.matlet.2012.02.025
47. D. Philip, C. Unni, S.A. Aromal, V.K. Vidhu, Murraya Koenigii leaf-assisted rapid green synthesis of silver and gold nanoparticles. Spectrochim. Acta A (2011). https://doi.org/10.1016/j.saa.2010.12.060
48. K. Roy, C.K. Sarkar, C.K. Ghosh, Photocatalytic activity of biogenic silver nanoparticles synthesized using yeast (*Saccharomyces cerevisiae*) extract. Appl. Nanosci. **5**, 953–959 (2015). https://doi.org/10.1007/s13204-014-0392-4
49. D. Ayodhya, G. Veerabhadram, Green synthesis, characterization, photocatalytic, fluorescence and antimicrobial activities of *Cochlospermum gossypium* capped Ag_2S nanoparticles. J. Photochem. Photobiol. B **157**, 57–69 (2016). https://doi.org/10.1016/j.jphotobiol.2016.02.002
50. C. Yu, L. Wei, W. Zhou, D.D. Dionysiou, L. Zhu, Q. Shu, H. Liu, A visible-light-driven core-shell like $Ag_2S@Ag_2CO_3$ composite photocatalyst with high performance in pollutants degradation. Chemosphere **157**, 250–261 (2016). https://doi.org/10.1016/j.chemosphere.2016.05.021
51. S.S. Muniandy, N.H. Mohd Kaus, Z.-T. Jiang, M. Altarawneh, H.L. Lee, Green synthesis of mesoporous anatase TiO_2 nanoparticles and their photocatalytic activities. RSC Adv. **7**, 48083–48094 (2017). https://doi.org/10.1039/C7RA08187A
52. Y. Xu, H. Xu, J. Yan, H. Li, L. Huang, Q. Zhang, C. Huang, H. Wan, A novel visible-light-response plasmonic photocatalyst CNT/Ag/AgBr and its photocatalytic properties. Phys. Chem. Chem. Phys. **15**, 5821 (2013). https://doi.org/10.1039/c3cp44104k
53. Y. Zang, R. Farnood, Photocatalytic activity of $AgBr/TiO_2$ in water under simulated sunlight irradiation. Appl. Catal. B **79**, 334–340 (2008). https://doi.org/10.1016/j.apcatb.2007.10.019
54. V. Vasanthakumar, A. Priyadharsan, P.M. Anbarasan, S. Muthumari, S. Subramanian, V. Raj, Enhancing toxic metal ions and dye removal properties of nanostructured terpolymer formed by diaminodiphenylmethane-resorcinol-formaldehyde. Chem. Select **2**, 9501–9510 (2017) https://doi.org/10.1002/slct.201700685